Journal of Materials Chemistry C

ROYAL SOCIETY OF CHEMISTRY

COMMUNICATION

View Article Online
View Journal | View Issue

Cite this: J. Mater. Chem. C, 2020, 8, 15092

Received 30th June 2020,
Accepted 4th August 2020

DOI: 10.1039/d0tc03078c

rsc.li/materials-c

Customizable and stretchable fibre-shaped electroluminescent devices *via* mulitcore-shell direct ink writing†

Dongna Liu,[abc] Jingbo Ren,[bc] Jizhe Wang,[bc] Wang Xing,[bc] Qilin Qian,[bc] Hangyu Chen[bc] and Nanjia Zhou *[bc]

One dimensional (1D) light-emitting fibres emerge as a top candidate for flexible and stretchable displays, enabling the miniaturization of device architectures and integration of different optoelectronic materials and components for new applications in textile- and human body-mounted, biomedical and bio-inspired optoelectronics. While conventional fabrication methods for 1D fibre-shaped devices typically involve multistep layer-by-layer coating processes, which are sophisticated and difficult to be directly integrated with wearable devices, 3D printing offers promise in the rapid integration of disparate functional materials within the printed filaments and facile patterning of 1D device architectures into 2D and 3D arbitrary form factors. Here for the first time, we demonstrate a universal, high throughput, and customizable printing method, known as multicore-shell direct ink writing (DIW) employing digital light processing (DLP)-printed printheads to simultaneously assemble different functional materials into 1D active device motifs. Using a 1D alternating current electroluminescent (ACEL) device as an example, we demonstrate the design and simultaneous printing of different electrodes, phosphors, and encapsulation inks, and the rapid prototyping of 1D ACEL fibres with high stretchability up to ~450%.

Introduction

The last few decades have witnessed the evolution of electronics from conventional rigid devices to highly soft and stretchable ones, enabling new applications in wearable electronics,[1–4] robotics,[5–7] and medical devices.[8–10] One embodiment of significant interest is the fibre-shaped light-emitting devices that can be miniaturized into a one-dimensional (1D) configuration and seamlessly integrated with textiles and human bodies to allow enhanced human/machine interfaces,[11] enabling new applications in textile displays,[12] sensors,[13] and camouflage.[14] Both fibre-shaped direct current (DC)-driven organic light-emitting diodes (OLEDs)/polymer light-emitting electrochemical cells (PLECs) and alternating current (AC)-driven electroluminescent devices have been demonstrated.[12,14–18] Compared to DC-driven OLED or PLEC fibres, ACEL devices offer potential compatibility with standard AC power sources and are relatively insensitive to geometry,[19] and therefore are excellent candidates for 1D stretchable light emitting fibres.

The conventional fabrication methods of 1D ACEL fibres with a basic device architecture of inner electrode/phosphor layer/outer electrode/encapsulation typically involve multistep layer-by-layer coating processes.[13,18,20–22] For the inner electrodes, either intrinsically conductive or silver nanowire (AgNW)-coated fibres are typically employed. Subsequently, a phosphor layer of a ZnS/elastomer composite is coated through spray-coating or dip-coating, followed by outer electrode integration, typically by the wrapping of, again, a 1D conductive nanomaterial such as AgNWs. Finally, for practical applications, an encapsulation layer is coated at the exterior. However, these approaches are sophisticated and difficult to be directly integrated with wearable devices. Besides, the uniform distribution of the functional materials around and along the fibres and solvent compatibility during the layer-by-layer sequential dipping process remain challenging. Recently, unlike using a conventional coaxial device architecture, a stretchable ACEL fibre with two inner parallel electrodes encapsulated within an outer phosphor layer has been developed by a coextrusion process to realize stretchable, twistable, and breathable textile displays.[14] Nevertheless, in their demonstration, the dual core-sheath architectures integrating only one kind of electrode and one phosphor layer material yield asymmetric distributions of the electric field within the phosphor layer and non-uniform luminance around the fibre circumference. It is highly desirable

[a] Zhejiang University, Hangzhou 310027, Zhejiang Province, China
[b] Key Laboratory of 3D Micro/Nano Fabrication and Characterization of Zhejiang Province, School of Engineering, Westlake University, 18 Shilongshan Road, Hangzhou 310024, Zhejiang Province, China. E-mail: zhounanjia@westlake.edu.cn
[c] Institute of Advanced Technology, Westlake Institute for Advanced Study, 18 Shilongshan Road, Hangzhou 310024, Zhejiang Province, China

† Electronic supplementary information (ESI) available. See DOI: 10.1039/d0tc03078c

to simultaneously incorporate different conductive, light-emitting, and encapsulating materials coaxially using a high throughput, highly customizable manufacturing method such as 3D printing to allow the versatile patterning of 1D fibres into 2D and 3D form factors. A recent example of structured multimaterial filaments incorporating pixelated light-emitting and light-detecting functions has been developed *via* a thermal drawing process, and a subsequent fused deposition modelling (FDM) printing process transforms the preformed rigid filaments into a wide range of hierarchical 3D objects.[23] However, the high temperature requirement and sophisticated parameter control during the thermal drawing and printing processes significantly constrain the choices of printable materials.

Here we report a new 3D printing method, known as multicore-shell direct ink writing, allowing the systematic ink design of different functional components for the fabrication of coaxially aligned ACEL devices with axially symmetric light emissions. Unlike the layer-by-layer coating and coextrusion methods, our multicore-shell DIW enables the one-step multimaterial integration and fabrication of 1D coaxially aligned multilayer optoelectronics, while at the same time allowing such devices to be patterned to form arbitrary 3D macrostructures with locally tunable light emissions. Additionally, unlike FDM methods, our ink-based printing also allows a comprehensive selection of functional materials and relatively mild processing conditions. Although core–shell DIW has been demonstrated previously for the manufacturing of bioscaffolds,[24] strain sensors,[25] and architected lattices,[26] these demonstrations are only limited to mechanical architectures or passive devices. We demonstrate for the first time, the multicore-shell DIW of active electronics. Our stretchable 1D ACEL fibres adopt a 4-layer device architecture. For the phosphor layer, we designed a printable ink based on a ZnS microparticle/dragon skin (DS) stretchable composite with tunable and bright emission colours.[5] We next designed a Ag/thermoplastic polyurethane (TPU) ink and a transparent, conductive ionic gel ink, as the inner and outer electrodes, respectively. Finally, a stretchable, transparent DS material is again employed as the encapsulation layer. By formulating all four inks with the proper rheological, electrical, light-emitting, and mechanical properties, we demonstrate the high throughput manufacturing of fibre-shaped ACEL devices with a high stretchability up to ~450%. With the ability to pattern 1D devices into complex arbitrary shapes, we designed and printed 1D, 2D, and 3D light-emitting architectures.

Results and discussion

To pattern the multicore-shell ACEL devices, we first designed and rapidly printed multicore-shell printheads employing commercially available high-resolution digital light processing (DLP) technique. The 4-layer tapered coaxial nozzles with a thickness of 200 μm for each channel are printed with high reproducibility. Each channel is connected to different syringes hosting different functional materials. The inner channels are slightly retracted to eliminate the effect of nozzle wall thickness at the output and improve the printing resolution (Fig. 1 and Fig. S1, ESI†).[26]

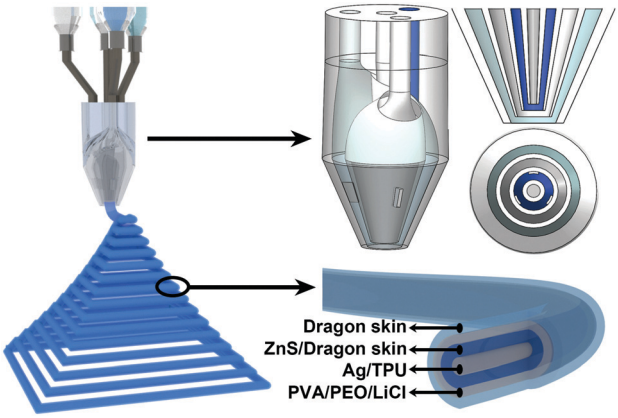

Fig. 1 Schematic illustration of the multicore-shell printheads and printed 1D stretchable ACEL devices.

Next we developed four viscoelastic inks for the stretchable ACEL fibres. Each of these inks is desirable to exhibit shear-thinning behaviour to ensure the simultaneous flow of all four materials and solid-like behaviour with sufficiently high storage modulus and yield stress to retain the overall cylindrical shapes after extrusion.[27] For the phosphor layer, inks are developed based on phosphor powders blended with an elastomeric material, DS. Commercially available phosphor powders including green light-emitting ZnS:Cu (ZnS:Cu(G)), blue light-emitting ZnS:Cu (ZnS:Cu(B)), and orange light-emitting ZnS:Cu, Mn with an average size of ~20 μm, ~20 μm and ~5 μm, respectively, were used as received (Fig. 2a and Fig. S2, ESI†). The overall phosphor ink design must consider several parameters such as printability, luminance, and strechability. By increasing the solid loading of ZnS:Cu(G) from 40 wt% to 70 wt%, the surface roughness of the cast films increases which is detrimental for smooth printing, and the aggregation of phosphor particles in the 70 wt% ZnS:Cu(G)/DS composite material limits its printability (Fig. 2a). Meanwhile, inks with a higher solid loading exhibit higher viscosity, storage and loss moduli (G' and G''), and yield stress (Fig. 2b and c). All inks exhibit a viscoelastic behaviour and high storage modulus, which are beneficial for printed structures to retain their cylindrical shapes after exiting from the printheads. We investigated the printability of the phosphor inks using standard metallic nozzles with an inner diameter of 200 μm (Fig. S3, ESI†), and all of the composites can be smoothly printed into the simple woodpile structures. Next, we compared the luminance (Fig. 2d) of 40 wt% and 60 wt% of ZnS:Cu(G)/DS composites using a 2D planar device architecture with a phosphor layer thickness of ~200 μm. As expected, increasing the phosphor particle content leads to enhanced light emission while slight decrease of the elongation at break (Fig. 2e). Therefore, considering the printability, luminance and mechanical properties, 60 wt% ZnS:Cu(G)/DS composite ink is selected as the phosphor layer.

We designed two electrode inks sandwiching the phosphor layer. For the inner electrode, we chose a Ag/TPU composite

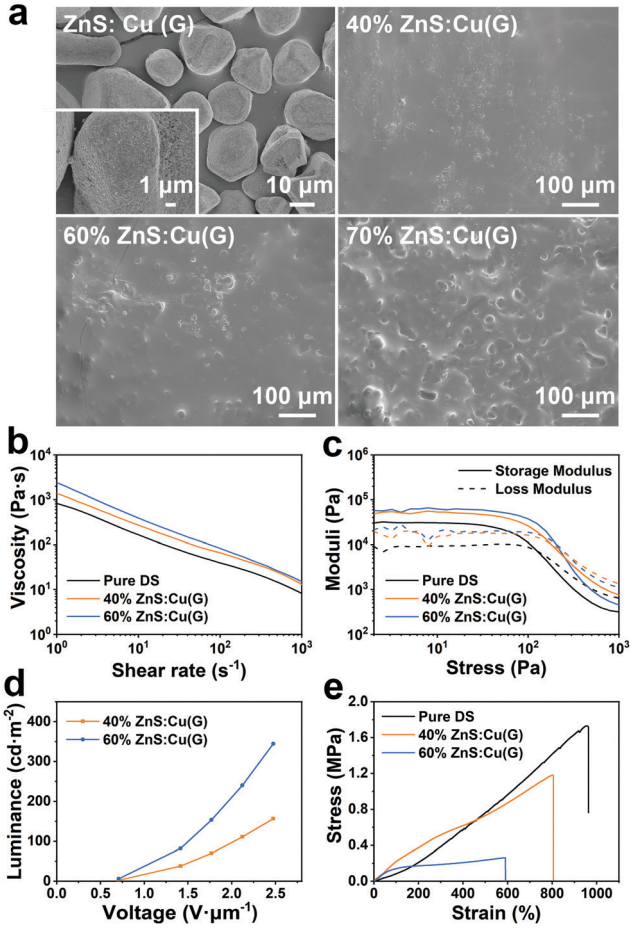

Fig. 2 Morphological, rheological, luminance and mechanical characterizations of the phosphor inks incorporating the green phosphor microparticle (ZnS:Cu(G)/DS) composite with different particle solid loadings. (a) SEM images of pristine ZnS:Cu (G) microparticles, cast films with 40 wt%, 60 wt%, and 70 wt% of ZnS:Cu(G)/DS composites. (b and c) Viscosity *vs.* shear rate, as well as storage (G') and loss (G'') moduli *vs.* stress for pure DS, 40 wt% and 60 wt% ZnS:Cu(G)/DS inks. (d) Comparisons of luminance of different thin film samples with 40 wt% and 60 wt% ZnS:Cu(G). (e) Tensile measurement of pure DS, 40 wt% and 60 wt% of ZnS:Cu(G) samples.

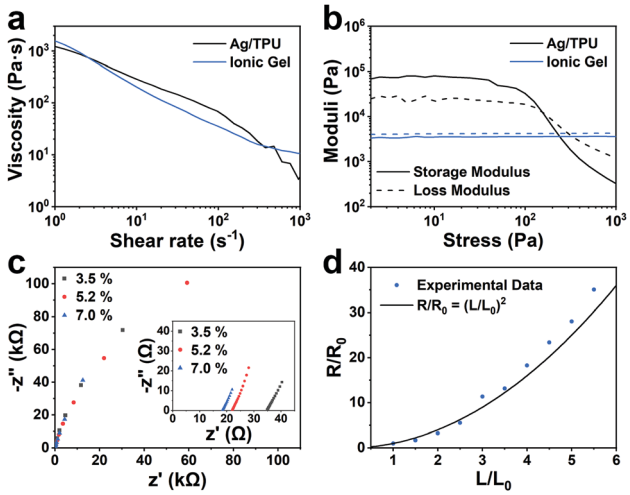

Fig. 3 Rheological and electrical properties of the electrode inks. (a and b) Rheological properties of the inner and outer electrode inks, Ag/TPU and ionic gel. The solid line and dashed line represent storage modulus and loss modulus, respectively. (c) Electrochemical impedance spectra of the ionic gels with different weight ratios of LiCl. (d) Change of resistance *vs.* strain of the dried 7.0 wt% of LiCl-based ionic gel samples.

which has been previously demonstrated for stretchable strain gauges.[28] As the outer electrode should be sufficiently transparent, inspired by the previous reports on highly stretchable conductive ionic gels, we developed a concentrated ionic gel-based ink composed of poly(vinyl alcohol) (PVA), poly(ethylene oxide) (PEO) and lithium chloride (LiCl) dissolved in deionized water (Table S1, ESI†).[5,14] Both of the two electrodes display an apparent shear-thinning behaviour (Fig. 3a) and the Ag/TPU composite ink demonstrates high plateau storage modulus and yield stress (Fig. 3b), which are sufficient to retain its cylindrical shape after extrusion. Although G'' of the outer electrode is slightly higher than G' (Fig. 3b), the printability and shape fidelity were unaffected due to its high viscosity, shear-thinning behaviour, and being encapsulated by the encapsulation layer. To explore the influence of LiCl salt concentration on the ionic conductivity of this ionic gel electrode, a series of composite materials with different LiCl contents were prepared and the corresponding electrochemical impedance spectra are shown in Fig. 3c. By increasing the LiCl concentration, the ionic conductivity increases from $\sim$0.029 S cm^{-1} for 3.5 wt% to $\sim$0.055 S cm^{-1} for 7.0 wt%, which is attributed to the increasing number of charge carriers.[29] Since it is difficult to evaluate the elongation of the viscous ionic gels, we instead measured samples after drying overnight which still display an impressive elongation of $\sim$1000% (Fig. S4, ESI†). The relationship between resistance and elongation is also recorded in Fig. 3d, and the predicted trend in eqn (1) is also shown alongside the measurement results:[30,31]

$$R/R_0 = (L/L_0)^2 \quad (1)$$

Finally, an elastomeric polymer, DS, is used as the encapsulation layer. Both the ionic gel and DS demonstrate decent optical transmittance (Fig. S5, ESI†). The detailed compositions of the four viscoelastic inks are listed in Table S1 (ESI†).

We next printed the complete ACEL fibres by simultaneously extruding all four inks (Fig. 4a left: longitudinal view; right: cross-sectional view). The thickness of each layer is controlled by adjusting the printing parameter and printhead structure. Under a high AC electric field, charge carriers trapped at the ZnS/DS interface are injected into the phosphor layer, and the injected electrons are accelerated to impact the luminescent centre or transported to the opposite ZnS/DS interface, leading to excitation or ionization of the luminescent centre. As a consequence, light emission occurs when the excess energy is released *via* radiative recombination.[32–34] The simple fibre-shaped ACEL device is fabricated to test the dependence of luminance on the applied electric fields (Fig. 4b). The luminance increases from 0.15 to 59.6 cd m^{-2} when the applied electric field intensity increases from 0.56 to 4.21 V μm^{-1} at a frequency of 3 kHz due to the increased number of charge

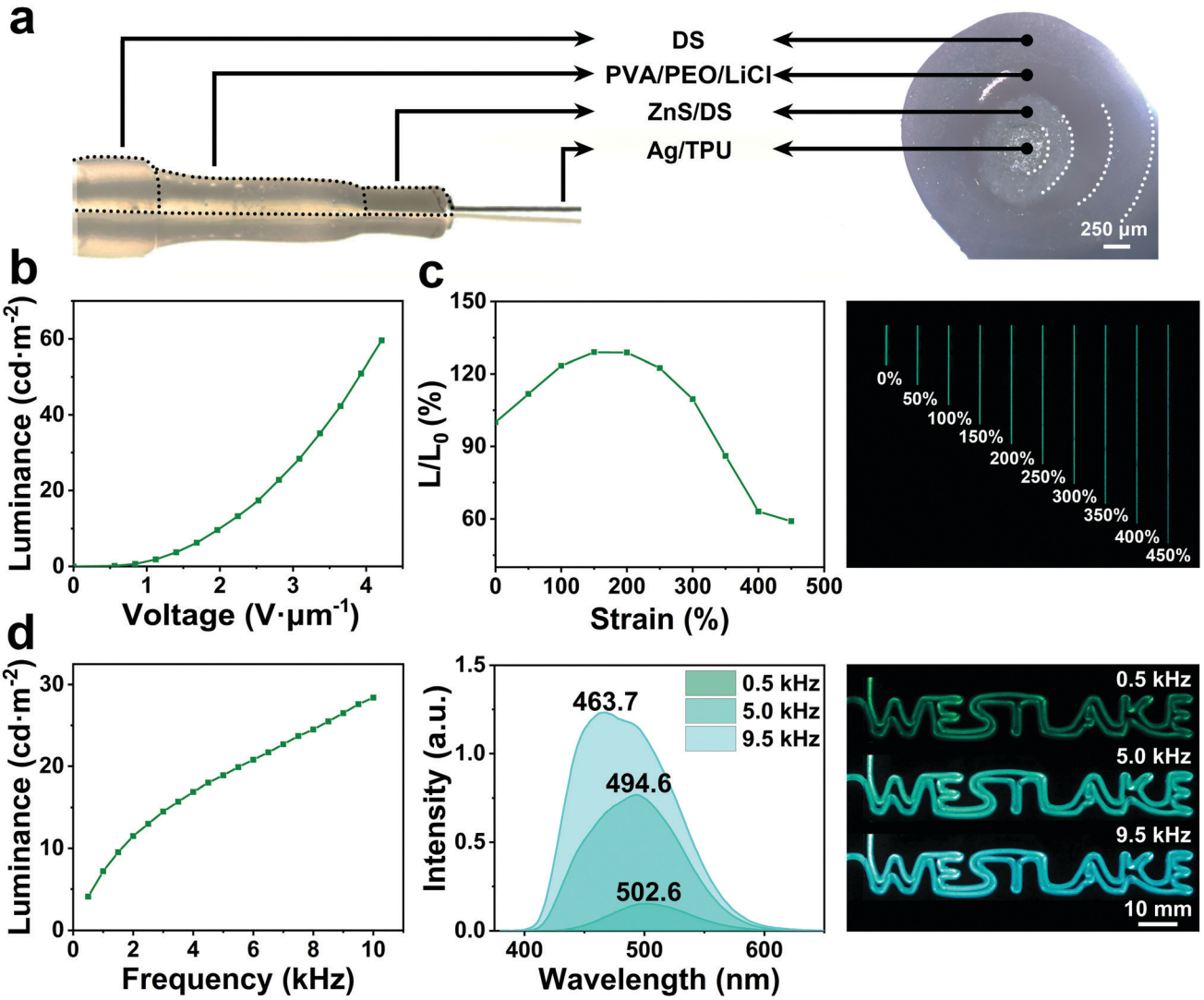

Fig. 4 Multicore-shell DIW of ACEL devices. (a) Photographs of the printed fibre with longitudinal and cross-sectional views. (b) Luminance–voltage relationship of the ACEL fibres with 60 wt% of phosphors measured at a constant frequency of 3 kHz. (c) Change of luminance (L/L_0) *vs.* strain of the printed ACEL fibres. (d) Luminance *vs.* frequency and the corresponding EL spectra of the ACEL fibres at a voltage of 380 V and photographs of "WESTLAKE" patterns under different frequencies of 0.5, 5.0, and 9.5 kHz.

carrier recombinations and excited luminescent centres. For a simple demonstration, we printed "WESTLAKE" showing uniform and bright luminescence (Fig. S6, ESI†). The luminance with different applied voltages follows the relationship in eqn (2):

$$L = L_0 \exp(-\beta/V^{1/2}) \quad (2)$$

where L is the luminance, V is the voltage, and L_0 and β are constants related to material properties.[35] We next measured the luminance of the printed devices subject to a uniaxial stretch. With increasing strain, the luminance first increased and then decreased, and the devices were found to be able to stretch up to ~450% without fail (Fig. 4c). The corresponding EL spectra were recorded (Fig. S7, ESI†). The increasing luminance at the beginning can be attributed to the enhanced electric field resulted from decrease in thickness of the phosphor layer after stretching (Fig. S8, ESI†). The degradation in luminance can be attributed to the decrease in the areal number density of phosphor particles (Fig. S9, ESI†) and the reduced conductivity of the two electrodes under large deformation.[18,33] Tensile measurement data (Fig. 2e and Fig. S4, ESI†) and optical images of ACEL devices under different strains (Fig. 4c) suggest the good adhesion between the four layers in the multicore-shell structure. Additionally, the relationship between luminance and frequency was also investigated (Fig. 4d). With increasing frequency, the luminance intensifies due to the enhanced electron–hole generation and luminescent centre excitation. The colour of the "WESTLAKE" pattern gradually changes from green to blue, and the corresponding peak wavelength shifts from ~502.6 nm to ~463.7 nm as the frequency increases from 0.5 kHz to 9.5 kHz. This phenomenon is a result of two emission bands in the ZnS material, namely, green emission and blue emission. The green emission at ~511 nm predominates at lower frequencies, which is related to the electron transfer between the impurity-induced

shallow defect state and the t_2 state of Cu. The blue emission at ~455 nm with higher energy excitation is more intense at higher frequencies. There exist various explanations about the blue emission, one of which is the transition between the conductive bands of ZnS and t_2 state of Cu.[36–40] Therefore, the phenomenon of blue shift was observed in the EL spectra with increasing frequency.

For our last demonstration, we printed ACEL devices with different phosphor layers incorporating ZnS:Cu(G), ZnS:Cu(B) and ZnS:Cu,Mn microparticles, showing different light-emitting colours and the arbitrary patterning of 1D fibres into 2D and 3D device architectures. The normalized EL spectra of ACEL devices with different colours are shown in Fig. 5a, and the peak wavelengths of the three light emissions are ~451.6, ~495.4 and ~586.4 nm, respectively. The corresponding chromaticity on the CIE (Commission on Illumination) 1931 diagram is plotted in Fig. 5b. Although we only demonstrate the ACEL devices with three distinct emission colours, a variety of wide-gap II–VI compounds doped with transition-metal or rare-earth luminescent centres can be employed to extend the chromaticity range.[41] The Chinese characters of "杭" with different colours including blue, green and orange were printed successfully to demonstrate that ACEL fibres with tunable light emission colours can be facially manufactured and integrated using our multicore-shell DIW approach (Fig. 5c, Video S1, and Table S2, ESI†). A stripe-like ACEL device embedded within the DS matrix was printed, exhibiting excellent mechanical compliance upon bending and twisting without suffering from luminance deterioration. Finally, a 3D pyramid-shaped ACEL device was conformally printed on an FDM-printed support to demonstrate the ability of our multicore-shell DIW technique to fabricate complicated and functional devices.

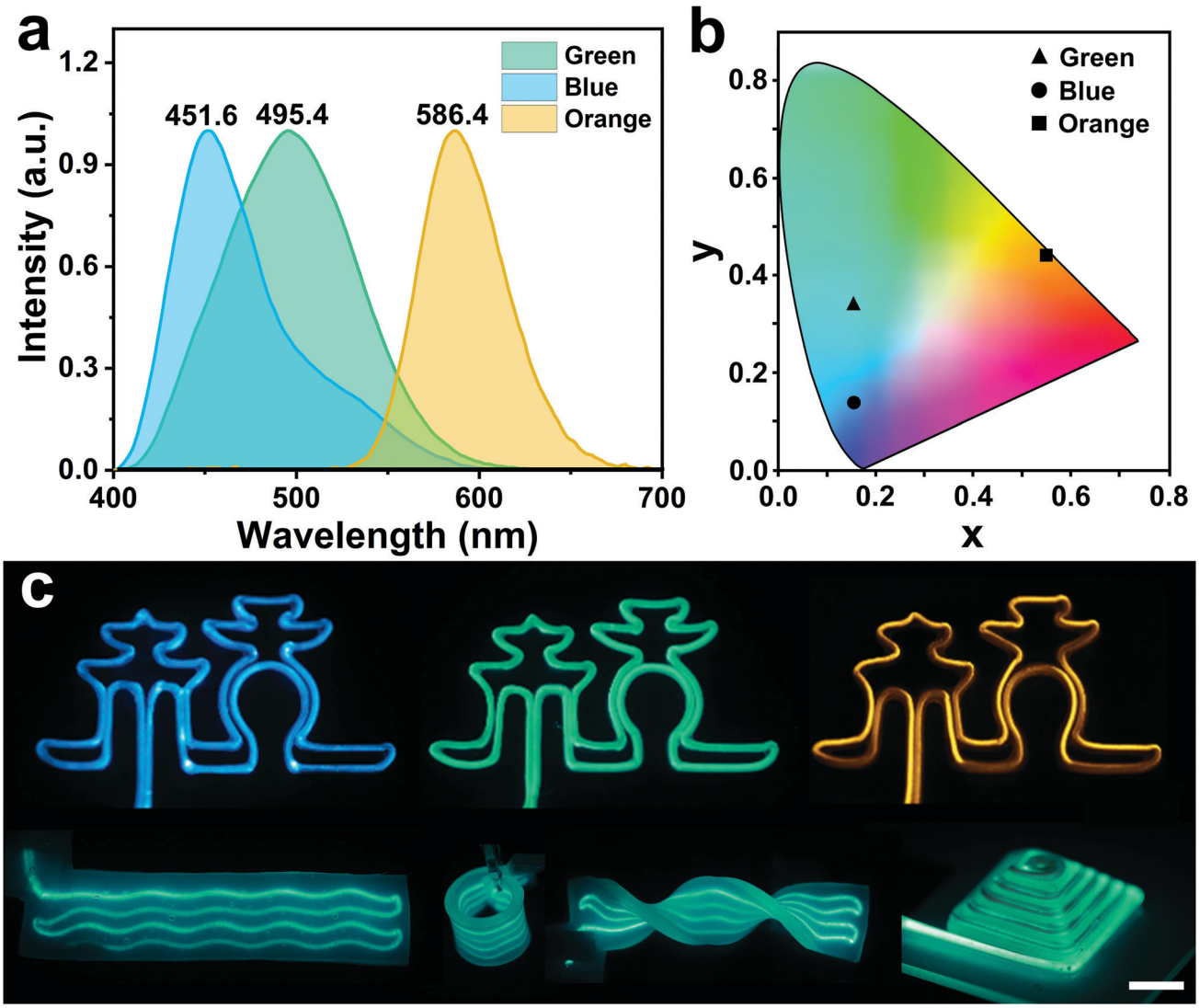

Fig. 5 Printed ACEL 1D, 2D and 3D fibres incorporating green, blue and orange-emitting ZnS microparticles. (a) Normalized EL spectra of ACEL devices incorporating ZnS:Cu(G), ZnS:Cu(B) and ZnS:Cu,Mn microparticles emitting green, blue, and orange colors and (b) the corresponding CIE1931 diagram. (c) Photographs of the printed ACEL devices with different structures and colors obtained from blue, green and orange light-emitting phosphors: Chinese characters of "杭", stripe under bending and twisting, and the 3D pyramid. The scale bar is 10 mm.

Conclusions

In summary, we demonstrate a novel one-step multicore-shell DIW method for manufacturing stretchable fibre-shaped ACEL devices. The careful design of the luminescent centers, electrodes and encapsulation inks, together with custom-printed printheads, enabled the simultaneous integration of these different functional materials within the 3D printed filaments. Our approach provides a universal, high-throughput, scalable and customizable manufacturing strategy for 1D optoelectronics. By the high-precision assembly of functional 1D devices into complex 3D macrostructures, our method would open new avenues for a variety of new applications such as portable energy-harvesting and storage devices, phototherapy and imaging bioelectronics, and wearable e-textiles.

Conflicts of interest

There are no conflicts to declare.

Acknowledgements

The authors are grateful for the financial support of this research by the National Natural Science Foundation of China (No. 51905446). The authors would like to acknowledge funding support from the Westlake University and Bright Dream Joint Institute for Intelligent Robotics.

Notes and references

1 J. Xu, S. Wang, G.-J. N. Wang, C. Zhu, S. Luo, L. Jin, X. Gu, S. Chen, V. R. Feig and J. W. To, *Science*, 2017, **355**, 59–64.
2 S. Wang, J. Xu, W. Wang, G.-J. N. Wang, R. Rastak, F. Molina-Lopez, J. W. Chung, S. Niu, V. R. Feig and J. Lopez, *Nature*, 2018, **555**, 83–88.
3 H. Wu, Y. Huang, F. Xu, Y. Duan and Z. Yin, *Adv. Mater.*, 2016, **28**, 9881–9919.
4 T. Q. Trung, S. Ramasundaram, B. U. Hwang and N. E. Lee, *Adv. Mater.*, 2016, **28**, 502–509.
5 C. Larson, B. Peele, S. Li, S. Robinson, M. Totaro, L. Beccai, B. Mazzolai and R. Shepherd, *Science*, 2016, **351**, 1071–1074.
6 N. Lu and D.-H. Kim, *Soft Robot.*, 2014, **1**, 53–62.
7 C. Zhang, S. Liu, X. Huang, W. Guo, Y. Li and H. Wu, *Nano Energy*, 2019, **62**, 164–170.
8 D.-H. Kim, N. Lu, R. Ghaffari, Y.-S. Kim, S. P. Lee, L. Xu, J. Wu, R.-H. Kim, J. Song and Z. Liu, *Nat. Mater.*, 2011, **10**, 316–323.
9 J. H. Koo, S. Jeong, H. J. Shim, D. Son, J. Kim, D. C. Kim, S. Choi, J.-I. Hong and D.-H. Kim, *ACS Nano*, 2017, **11**, 10032–10041.
10 D. Qi, Z. Liu, M. Yu, Y. Liu, Y. Tang, J. Lv, Y. Li, J. Wei, B. Liedberg and Z. Yu, *Adv. Mater.*, 2015, **27**, 3145–3151.
11 S. Kwon, Y. H. Hwang, M. Nam, H. Chae, H. S. Lee, Y. Jeon, S. Lee, C. Y. Kim, S. Choi and E. G. Jeong, *Adv. Mater.*, 2020, **32**, 1903488.
12 S. Kwon, H. Kim, S. Choi, E. G. Jeong, D. Kim, S. Lee, H. S. Lee, Y. C. Seo and K. C. Choi, *Nano Lett.*, 2018, **18**, 347–356.
13 X. Zhou, X. Xu, Y. Zuo, M. Liao, X. Shi, C. Chen, S. Xie, P. Zhou, X. Sun and H. Peng, *J. Mater. Chem. C*, 2020, **8**, 935–942.
14 Z. Zhang, L. Cui, X. Shi, X. Tian, D. Wang, C. Gu, E. Chen, X. Cheng, Y. Xu, Y. Hu, J. Zhang, L. Zhou, H. H. Fong, P. Ma, G. Jiang, X. Sun, B. Zhang and H. Peng, *Adv. Mater.*, 2018, **30**, 1800323.
15 K.-J. Ko, H. B. Lee, H. M. Kim, G. J. Lee, S.-R. Shin, N. Kumar, Y. M. Song and J.-W. Kang, *Nanoscale*, 2018, **10**, 16184–16192.
16 Z. Zhang, K. Guo, Y. Li, X. Li, G. Guan, H. Li, Y. Luo, F. Zhao, Q. Zhang, B. Wei, Q. Pei and H. Peng, *Nat. Photonics*, 2015, **9**, 233–238.
17 Z. Zhang, Q. Zhang, K. Guo, Y. Li, X. Li, L. Wang, Y. Luo, H. Li, Y. Zhang, G. Guan, B. Wei, X. Zhu and H. Peng, *J. Mater. Chem. C*, 2015, **3**, 5621–5624.
18 D. Hu, X. Xu, J. Miao, O. Gidron and H. Meng, *Materials*, 2018, **11**, 184.
19 L. Wang, X. Fu, J. He, X. Shi, T. Chen, P. Chen, B. Wang and H. Peng, *Adv. Mater.*, 2020, **32**, 1901971.
20 G. Liang, M. Yi, H. Hu, K. Ding, L. Wang, H. Zeng, J. Tang, L. Liao, C. Nan and Y. He, *Adv. Electron. Mater.*, 2017, **3**, 1700401.
21 Z. Zhang, X. Shi, H. Lou, X. Cheng, Y. Xu, J. Zhang, Y. Li, L. Wang and H. Peng, *J. Mater. Chem. C*, 2018, **6**, 1328–1333.
22 T. Sun, F. Xiu, Z. Zhou, C. Ban, T. Ye, Y. Ding, J. Liu and W. Huang, *J. Mater. Chem. C*, 2019, **7**, 1472–1476.
23 G. Loke, R. Yuan, M. Rein, T. Khudiyev, Y. Jain, J. Joannopoulos and Y. Fink, *Nat. Commun.*, 2019, **10**, 1–10.
24 N. Raja and H.-s. Yun, *J. Mater. Chem. B*, 2016, **4**, 4707–4716.
25 A. Frutiger, J. T. Muth, D. M. Vogt, Y. Menguc, A. Campo, A. D. Valentine, C. J. Walsh and J. A. Lewis, *Adv. Mater.*, 2015, **27**, 2440–2446.
26 J. Mueller, J. R. Raney, K. Shea and J. A. Lewis, *Adv. Mater.*, 2018, **30**, 1705001.
27 Q. Chen, J. Zhao, J. Ren, L. Rong, P. F. Cao and R. C. Advincula, *Adv. Funct. Mater.*, 2019, **29**, 1900469.
28 A. D. Valentine, T. A. Busbee, J. W. Boley, J. R. Raney, A. Chortos, A. Kotikian, J. D. Berrigan, M. F. Durstock and J. A. Lewis, *Adv. Mater.*, 2017, **29**, 1703817.
29 E. H. Cha, S. A. Lim, C. W. Lee and D. R. Macfarlane, *J. Power Sources*, 2006, **163**, 269–273.
30 C. Keplinger, J.-Y. Sun, C. C. Foo, P. Rothemund, G. M. Whitesides and Z. Suo, *Science*, 2013, **341**, 984–987.
31 C.-C. Kim, H.-H. Lee, K. H. Oh and J.-Y. Sun, *Science*, 2016, **353**, 682–687.
32 W. A. D. M. Jayathilaka, A. Chinnappan, J. N. Tey, J. Wei and S. Ramakrishna, *J. Mater. Chem. C*, 2019, **7**, 5553–5572.
33 J. Wang, C. Yan, K. J. Chee and P. S. Lee, *Adv. Mater.*, 2015, **27**, 2876–2882.
34 L. Wen, N. Liu, S. Wang, H. Zhang, W. Zhao, Z. Yang, Y. Wang, J. Su, L. Li, F. Long, Z. Zou and Y. Gao, *Opt. Express*, 2016, **24**, 23419–23428.
35 P. Zalm, *Philips Res. Rep.*, 1956, **11**(353–399), 417–451.

36 S. Xu, S. Chua, B. Liu, L. Gan, C. Chew and G. Xu, *Appl. Phys. Lett.*, 1998, **73**, 478–480.
37 W. Peng, G. Cong, S. Qu and Z. Wang, *Opt. Mater.*, 2006, **29**, 313–317.
38 S. Ummartyotin, N. Bunnak, J. Juntaro, M. Sain and H. Manuspiya, *Solid State Sci.*, 2012, **14**, 299–304.
39 C. D. Brubaker, K. N. Newcome, G. K. Jennings and D. E. Adams, *J. Mater. Chem. C*, 2019, **7**, 5573–5578.
40 K. Park, H. Jeong, J. Park, G. Deressa, Y. Jeong, K. Lim, S. Lee and J. Kim, *J. Lumin.*, 2015, **165**, 216–219.
41 H. Kobayashi and S. Tanaka, *J. Soc. Inf. Disp.*, 1996, **4**, 157–164.